NOTE

Realization of a push-me-pull-you swimmer at low Reynolds numbers

To cite this article: O Silverberg *et al* 2020 *Bioinspir. Biomim.* **15** 064001

Bioinspiration & Biomimetics

Note

Realization of a push-me-pull-you swimmer at low Reynolds numbers

RECEIVED
14 April 2020

REVISED
11 June 2020

ACCEPTED FOR PUBLICATION
3 July 2020

PUBLISHED
11 September 2020

O Silverberg[1], E Demir[1,2], G Mishler[1], B Hosoume[1], N Trivedi[1], C Tisch[1], D Plascencia[3], O S Pak[1,4] and I E Araci[2,4]

[1] Department of Mechanical Engineering, Santa Clara University, 500 El Camino Real, CA 95053, United States of America
[2] Beijing Computational Science Research Center, Beijing 100193, China
[3] Department of Bioengineering, Santa Clara University, 500 El Camino Real, CA 95053, United States of America
[4] Authors to whom any correspondence should be addressed.

E-mail: opak@scu.edu and iaraci@scu.edu

Keywords: low-Reynolds-number swimmers, microswimmers, locomotion

Supplementary material for this article is available online

Abstract

Locomotion at low Reynolds numbers encounters stringent physical constraints due to the dominance of viscous over inertial forces. A variety of swimming microorganisms have demonstrated diverse strategies to generate self-propulsion in the absence of inertia. In particular, ameboid and euglenoid movements exploit shape deformations of the cell body for locomotion. Inspired by these biological organisms, the 'push-me-pull-you' (PMPY) swimmer (Avron J E *et al* 2005 *New J. Phys.* **7** 234) represents an elegant artificial swimmer that can escape from the constraints of the scallop theorem and generate self-propulsion in highly viscous fluid environments. In this work, we present the first experimental realization of the PMPY swimmer, which consists of a pair of expandable spheres connected by an extensible link. We designed and constructed robotic PMPY swimmers and characterized their propulsion performance in highly viscous silicone oil in dynamically similar, macroscopic experiments. The proof-of-concept demonstrates the feasibility and robustness of the PMPY mechanism as a viable locomotion strategy at low Reynolds numbers.

1. Introduction

Biological organisms adopt diverse strategies to swim across different length scales [1–3], from swimming microorganisms such as bacteria to fishes and mammals such as blue whales [4]. The physics of swimming involves a complex interplay between the body actuation of the swimmer and the induced flow in its surrounding fluid. The Reynolds number, $\mathrm{Re} = \rho UL/\mu$, characterizes the relative importance of inertial to viscous forces in a swimming problem, for a swimmer with a characteristic length L and speed U in a fluid with density ρ and dynamic viscosity μ. Macroscopic aquatic animals typically reside in the high Reynolds number regime and use inertia in their locomotion. Swimming under the microscope, on the other hand, occurs at low Reynolds number, where viscous forces dominate inertial effects. Consider a bacterium with size 10 μm swimming at a speed 30 μm s^{-1} in water, the Reynolds number is on the order of 10^{-4}. Inertia is thus negligible, rendering macroscopic mechanisms that rely on inertia, such as rigid flapping motion, ineffective in propelling swimmers in the microscopic world. Purcell's scallop theorem shows that any reciprocal motion cannot generate self-propulsion at low Re [5, 6]. The absence of inertia imposes a fundamental challenge on effective locomotion strategies in this physical regime, which has attracted substantial interests across different disciplines of science and engineering [7–10]. The hydrodynamics of cell motility is not only important for its fundamental role in physics and biology; it has also attracted considerable, recent attention due to its potential applications in designing artificial microswimmers for medical tasks, such as targeted drug delivery and microsurgery [11–13].

The biological world has shown us different strategies to swim in the absence of inertia. Some spermatozoa and bacteria swim by bending or rotating their slender appendages called flagella [14, 15]. The drag anisotropy of slender structures like flagella allows these flagellated microorganisms to manip-

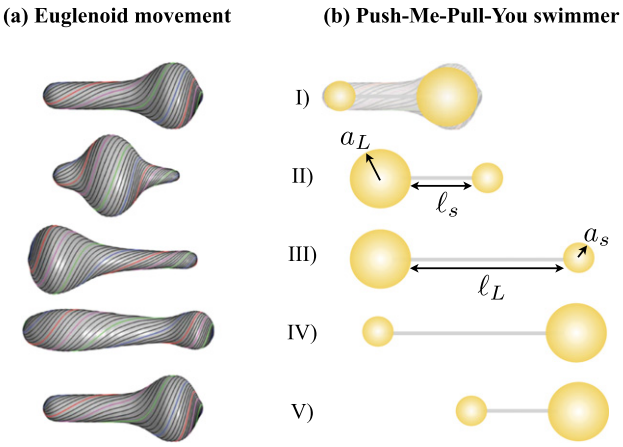

Figure 1. (a) Reconstructions of the euglenoid movement (from top to bottom) based on video recordings of euglenids [27]. (b) The sequence of shape changes for a PMPY swimmer and notations [28].

ulate viscous drag for generating propulsive thrust. Flagellar beating of spermatozoa has inspired the development of artificial flexible flagella [16–18]. Another type of biomimetic microswimmers adopts the helical structures of bacterial flagella for propulsion [19, 20]. These artificial propellers rely on the presence of external magnetic fields for actuation. As a remark, a genuine low-Re swimmer should be both free of force and torque [15, 21]. While these magnetically actuated structures are force-free, they are not torque-free due to the externally imposed magnetic torques. These structures, hence, do not qualify as swimmers and should be more appropriately termed propellers [18, 22]. Examples of low-Re swimmers include chemical swimmers such as auto-diffusiophoretic and auto-electrophoretic particles. These phoretic swimmers convert chemical energy to mobility by the generation of local gradients of solute concentration or electrical potential via asymmetric surface activity [23]. Although their locomotion does not rely on external magnetic fields, the presence of chemical fuels such as hydrogen peroxide is typically required, which could limit their medical applications in practical scenarios.

Another class of low-Re swimmers exploit shape deformations for locomotion. While amoeboid locomotion is more commonly known for crawling on solid surfaces, recent studies have showed that some amoebae and neutrophils can swim by similar body distortions [24–26]. As another notable example, some euglenids execute large-amplitude deformations of the entire cell in a concerted fashion, known as euglenoid movement or metaboly (figure 1(a)). The euglenoid movement has been shown to be a viable method of swimming, with a hydrodynamic efficiency comparable with that by flagellar and ciliary propulsion [27]. Overall, the versatility of locomotion via shape deformations in traversing both solid and fluid terrains is highly desirable for artificial microswimmers, which need to navigate complex and varying biological environments in their medical applications.

The euglenoid movement has inspired the design of an artificial microswimmer known as the push-me-pull-you (PMPY) swimmer by Avron *et al* [28]. The PMPY swimmer may be considered as a discretized version of the continuous euglenoid movement, where the shape deformation is implemented through a pair of deformable spheres that change their volumes and separation distance. Figure 1(b) displays the sequence of deformation, which resembles the euglenoid movement (figure 1(a)). The propulsion mechanisms may be understood intuitively as follows: in step I $\rightarrow$ II, the expanding sphere acts as a source that pushes away the contracting sphere, which acts as a sink to pull the expanding sphere (hence the name, PMPY [28]). Such PMPY mechanism results in a net displacement in the direction of the contracting sphere; note that the same mechanism is at play in step III $\rightarrow$ IV, but the net displacement is expected to less pronounced when the spheres are further apart. Next, in step II $\rightarrow$ III in the sequence, where the link between the spheres extends, the larger sphere serves as an anchor to allow a greater reach of the smaller sphere, resulting in a net displacement in the direction of the smaller sphere again. As a result of kinematic reversibility at low Reynolds numbers, when the link contracts in step IV $\rightarrow$ V, the same net displacement occurs but in the direction of the larger sphere; yet, since the larger sphere is on the right-hand side, the net displacement is towards the right. This sequence of shape changes, therefore, leads to an overall swimming motion towards the right.

The first use of reconfigurable linked-spheres for locomotion at low Re was pioneered by Golestanian & Najafi's three-sphere swimmer [29], which consists of three rigid spheres connected by two extensible links. The simplicity and elegance of the design has since attracted considerable attention [30–35]. By allowing expansion and contraction of the spheres,

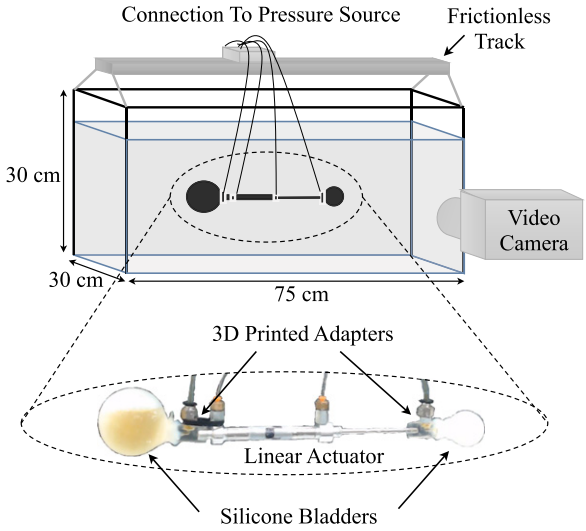

Figure 2. Schematic of the experimental set up (top) and of the fabricated PMPY swimmer (bottom) immersed in a bath of high viscosity silicone oil.

the PMPY mechanism requires only two spheres and one extensible link, which is even conceptually simpler and more efficient than the three-sphere swimmer [28, 36]. While the three-sphere swimmer has been realized using various macroscopic and microscopic experimental platforms [37–40], the bioinspired PMPY mechanism has not been experimentally implemented to the best of our knowledge.

In this work we present the first experimental realization of the PMPY swimmer at low Re. To maintain dynamic similarity with a low-Re environment, a macroscopic robotic swimmer based on the PMPY mechanism was immersed in a highly viscous silicone oil. The use of dynamically similar, macroscale robotic swimmers has been effective for investigating different propulsion mechanisms at low Re, including elastohydrodynamic [41, 42] and helical [43–46] propulsion, among others [47–51]. In the same spirit, we present here a macroscopic realization of the bioinsipred PMPY swimmer as a proof-of-concept. The structure of the paper is as follows. We first present the fabrication process and experimental design in section 2. Next, we discuss the performance characterization of the PMPY swimmers in section 3, before some concluding remarks on potential future miniaturization in section 4.

2. Fabrication and experimental design

To realize the PMPY mechanism shown in figure 1(b), two elastomeric spheres were fabricated by the silicone molding process. First, the molds were 3D printed using polylactic acid. No extra treatment was applied after the printing. EcoFlex 00-30 (Smooth-On Inc.) was chosen as the elastomeric material due to its high elongation before break value (900%) and low Young's modulus (69 kPa). These features enabled large radial expansions (up to 300%) with small input pressures in the range of 100–140 kPa. The pneumatic linear actuator (Original Line, Bimba Inc.) was used as the central rod, due to its accuracy, repeatability and ease of use. A schematic of the experimental setup is shown in figure 2.

Three PMPY swimmers were fabricated with identical elastomeric spheres with an undeformed radius of 3.8 cm and different linear actuator stroke lengths ($\Delta\ell = \ell_L - \ell_s$) of 4.8 cm, 8.6 cm, and 12.9 cm. The volume change of the spheres affects their buoyant forces, which would cause vertical displacement and tilting of the swimmer. These buoyancy fluctuations represent sources of noise in our measurements and may contribute to deviations from theoretical predictions assuming neutral buoyancy. We minimized these effects by filling the spheres with water, whose density is closer to that of the silicon oil. This also reduced the force on the tubing attached to a frictionless track (Neewer 23.6 inch) above the tank, as shown in figure 2. To supply pressure, the elastomeric spheres with a single pressure input were connected to three-way two-position solenoid valves (1/4″, USSOLID) and the linear actuator was connected to a five-way two-position solenoid valve (1/4″, USSOLID). A five-way valve was required for the linear actuator because of the two chambers (i.e., separate chambers are used for extension and retraction) that need to be actuated in the double-acting linear actuator. The connection between the PMPY and the valves were established through Tygon tubing (1/8″ inner diameter). An input pressure of 138 kPa was used to pressurize both the spheres and the linear actuator. As shown in figure 2, 3D printed adapters allow the attachment of the spheres to the linear actuator while providing connections for pneumatic tubing. The valve's on/off states were controlled via an Arduino Uno.

We immersed the swimmers in a bath of high viscosity (100 000 cSt) silicone oil (Elkay Silicones

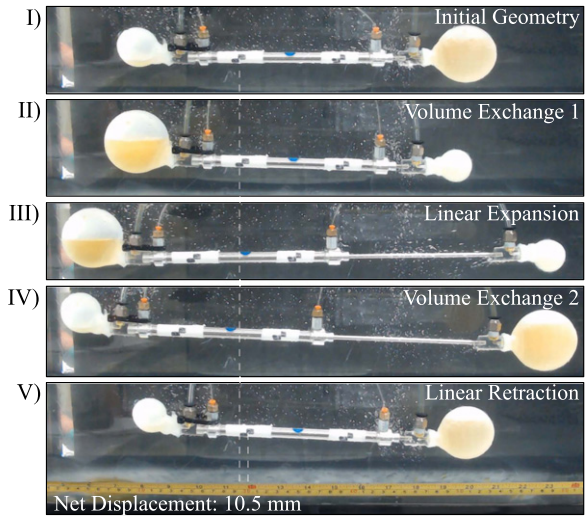

Figure 3. Implementation of the full swimming cycle of swimmer with a stroke length of 12.9 cm according to the five steps shown in figure 1(b). The net displacement was measured to be 10.5 mm to the right.

LK-SIL 100T-100K) and used slow actuation rates for the pneumatic cylinder and spheres to maintain a low-Re environment. Typical Reynolds numbers in the experiments are on the order of 0.1. Spheres were expanded to varying radial expansion ratios, $R = a_L/a_s$, by modifying their inflation and deflation durations. A webcam (C922 1080p, Logitech Inc.) was used to record the movement of the swimmers. Computer vision toolbox of MATLAB was utilized to track the PMPY swimmer. This was realized via the corner function where the high contrast area on the swimmer was selected and tracked automatically throughout the subsequent frames. The displacement of the swimmer and the diameters of the spheres were measured by converting the number of pixels into physical lengths from recorded videos of the experiments.

3. Results and discussion

In figure 3, we show a robotic PMPY swimmer executing the sequence of motion depicted in figure 1(b) in a typical experiment. After completing a full swimming cycle, the swimmer obtained a net positive displacement to the right. See also a supplementary video for the motion of the PMPY swimmer (available online at stacks.iop.org/JPhysBB/15/064001/mmedia). We measured the net displacement per cycle of the PMPY swimmer (X) at varying expansion ratios (R) and stroke lengths ($\Delta\ell$). As shown in figure 4, for a given stroke length, as the expansion ratio R is increased, an increase in displacement per cycle X is evident. Also, by increasing the stroke length of the swimmer $\Delta\ell$, a more dramatic increase in displacement per cycle is observed.

We compare our experimental measurements with predictions by a simple theoretical model based on the superposition of the solutions to the Stokes equation for two deforming spheres [28]. When the hydrodynamic interactions between the spheres are ignored and assuming large expansion ratios, the net displacement of a PMPY swimmer is given by $X = K(R-1)\Delta\ell/(R+1)$, for a given expansion ratio R and stroke length $\Delta\ell$ (see appendix A for more details on the theoretical model), and K is a scale factor we insert to obtain the best fit between our experimental measurements and the formula. We found that a scale factor of $K = 0.3$ provides reasonable fittings between the experimental measurements (symbols) and scaled theoretical prediction (dashed lines), as shown in figure 4(a). Consistent with our experimental measurements, the model predicts more substantial enhancement in the net displacement of the swimmer due to increase in stroke length than increase in the radial expansion ratio. Furthermore, by non-dimensionalizing the net displacement by the stroke length, i.e., $X/\Delta\ell = K(R-1)/(R+1)$, data with different expansion ratios and stroke lengths (symbols) all collapse onto a single curve as predicted by the theory and observed in figure 4(b) (dashed line). These results demonstrate the effectiveness of the theoretical model in capturing the essential swimming characteristics of the PMPY swimmer.

We discuss the limitations in the comparison of our experiments with the theoretical model. The experiments measured consistently lower values of the net displacement compared with the model's predictions, as indicated by the small scale factor K of 0.3. There are several effects ignored in the theoretical model, which could either increase or decrease the net displacement of the swimmer. First, we consider the effect of hydrodynamic interaction between the spheres. The original model by Avron *et al* assumed the spheres to be infinitely apart and thus ignored any hydrodynamic interaction. More recently, Wang

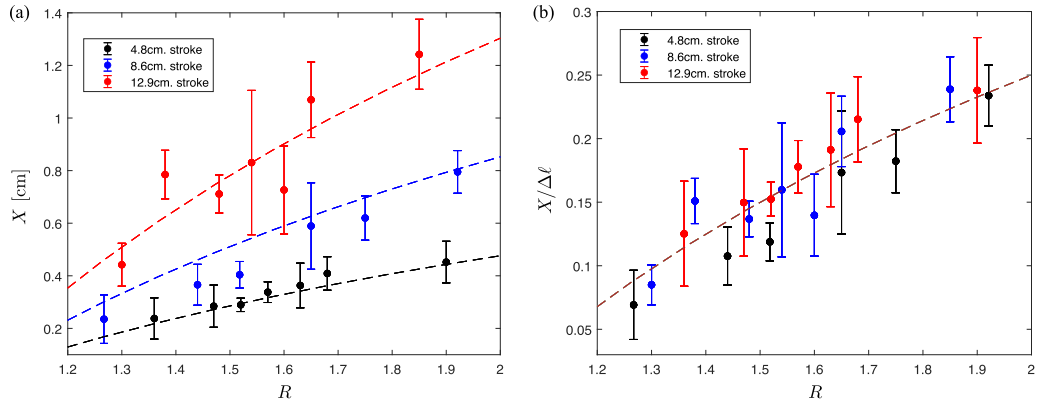

Figure 4. (a) Net displacement per cycle, X, as a function of the radial expansion ratio of the spheres, $R = a_s/a_L$. The dashed lines represent the best fits with the theoretical predictions with a scale factor $K = 0.3$ for $\Delta\ell = 4.8$ cm (black), 8.6 cm (blue), and 12.9 cm (red). (b) Dimensionless net displacement per cycle scaled by the stroke length, $X/\Delta\ell$, as a function of the radial expansion ratio, a. The dashed line represents the best fit with theoretical prediction with a scale factor $K = 0.3$. In these experiments, for each expansion ratio of the spheres, the swimmers were actuated for three cycles to obtained the average net displacement per cycle. The standard deviation of the ten trials for each expansion ratio is provided as the error bars.

& Othmer [52] calculated the higher-order corrections due to the interaction between the spheres in the PMPY model. Based on their results, considering a typical setup with $R = \ell_L/\ell_s = 2$ and $\Delta\ell = 10a_s$, we estimated the leading-order correction to the net displacement (see equation (A.8) in appendix A), $3a_sR\ln(\ell_L/\ell_s)/(R+1)\Delta\ell$, to increase the net displacement by approximately 14%. We thus argue that the observed reduction in net displacement may not be attributed to the hydrodynamic interaction between the spheres.

Next we turn to the effect due to the presence of the connecting rod, which was also ignored in the theoretical model. In particular, the dead side of the pneumatic cylinder (the portion with cylinder barrel) always contributes additional drag at the rear end of the swimmer throughout the swimming cycle. Such an additional drag component modifies the asymmetry in drag distribution on the swimmer, affecting the swimmer's net displacement. By modeling the dead portion of the pneumatic cylinder (with length ℓ_s) as an elongated rod, the drag on this portion can be estimated as $D_c = 2\pi\mu\ell_s U/[\ln(\ell_s/b) - 1/2]$ when the cylinder moves axially at speed U, where b is the radius of the cylinder [53]. With typical geometrical values in the experiment ($\ell_s/a_s = 10$ and $\ell_s/b = 40$), we estimated that the drag due to the cylinder could be comparable to the drag on the smaller sphere in our experiment. This additional drag component at the rear end is hence not negligible, which would alter the swimmer's displacement in different manners depending on the specific stroke. As a crude estimate of its overall effect on the net displacement, we lump this additional drag $D_c \approx 6\pi\mu a_s U$ together with the drag on the rear sphere, which may be considered as increasing the effective size of the rear sphere throughout the cycle in effect. For instance, consider an original expansion ratio $R = a_L/a_s = 2$, the additional drag due to cylinder would increase the effective size of the rear sphere from $2a_s$ to $3a_s$ in step II $\rightarrow$ III and from a_s to $2a_s$ in step IV $\rightarrow$ V, causing an overall reduction in the swimmer's net displacement by approximately 24%. While this effect represents a plausible source contributing to the lower values of measured net displacement, we note that the reduction was more significant in the experiment. There are other factors, including the drag on the pneumatic tubing and the asymmetric tension the tubing exerts on the swimmer, that could also restrain the swimmer's movement. In addition, we defer the analysis of the confinement effects to future numerical simulations due to the simultaneous presence of multiple and distinct types of confining surface (free and solid surfaces) in our experiment. These various factors arising in the practical implementation may contribute to the observed departure from predictions from the simple theoretical model.

4. Concluding remarks

Inspired by the euglenoid movement, the PMPY swimmer proposed by Avron *et al* [28] represents an elegant self-propulsion mechanism at low Reynolds numbers. We present in this work the first realization of the PMPY mechanism via a dynamically similar, macroscopic experimental setup. We designed and fabricated robotic PMPY swimmers and characterized their performance in highly viscous silicone oil. Despite various practical complexities not considered in the original model, this proof-of-concept demonstrated the feasibility and robustness of the bioinspired mechanism in generating self-propulsion at low Reynolds numbers.

We remark on potential ways of designing miniaturized and untethered PMPY swimmers, which requires sufficient and controllable power for soft

sphere expansion and the linear actuation at small scales. Swimmers consisting of rigid spheres with variable separation distances have already been realized experimentally with various techniques, including optical tweezers [37] or external magnetic fields [38–40]. The challenge of realizing untethered and deformable spheres at small scales may be tackled with the use of soft active materials such as hydrogels [54, 55] and liquid-crystal elastomers [56]. These novel materials exhibit configurational changes in response to heat or light, representing a promising class of actuation mechanisms for reconfigurable microscopic swimmers [57, 58]. Finally, the integration of such reconfigurable systems with machine learning techniques presents a new path towards realizing adaptive (or "smart") swimmers for robust locomotion in complex environments [61, 62, 63].

Acknowledgments

The authors thank Andrew Torrance, Jonathan Borst, and Matthew Holmes for assistance in the experimental setup and Professor Yong Lin Kong for useful discussion. This work was supported by the National Science Foundation Grant 1830958 (to OSP).

Appendix A. Theoretical model of the PMPY swimmer

We include in this appendix some key steps in arriving at the theoretical results of the PMPY swimmer discussed in the main text. More details can be found in the original work by Avron *et al* [28] and subsequent analyses on this model swimmer [36, 52].

We denote the radius of the two spheres as $a_i(t)$, where $i = 1, 2$ and t represents time, and the distance between the center of the spheres as $\ell(t)$. When the spheres are assumed to be infinitely apart for hydrodynamic interaction to be ignored, the velocities U_i and forces F_i on spheres 1 and 2 are related as

$$U_1 = \frac{F_1}{6\pi\mu a_1} + \frac{a_1^2}{\ell^2}\dot{a}_1, \tag{A.1}$$

$$U_2 = \frac{F_2}{6\pi\mu a_2} + \frac{a_2^2}{\ell^2}\dot{a}_2, \tag{A.2}$$

in Stokes flows. Here the first terms, $F_i/(6\pi\mu a_i)$, and second terms, $a_i^2\dot{a}_i/\ell^2$, on the right hand of the above equations, respectively, capture the effect of translation and radial expansion of the sphere [53, 59]. The velocities are also related by the kinematics of the connecting rod as $U_2 - U_1 = \dot{\ell}$. By enforcing the force-free condition for the swimmer, $F_1 + F_2 = 0$, the instantaneous velocity of the swimmer, $\bar{U} = (U_1 + U_2)/2$, is given by

$$\bar{U} = \frac{a_1 - a_2}{2(a_1 + a_2)}\dot{\ell} + \frac{a_1^2}{\ell^2}\dot{a}_1. \tag{A.3}$$

Upon integration of the velocity over time in the strokes described in figure 1(b) for one cycle, the net displacement of the swimmer is given by

$$X = \frac{a_L - a_s}{a_L + a_s}(\ell_L - \ell_s) = \frac{R-1}{R+1}\Delta\ell. \tag{A.4}$$

As expected for locomotion at Re, the net displacement per cycle of a swimmer is independent of its rate but only the sequence of shape changes [5, 60]. We remark that while the net displacement per cycle is rate-independent, the speed of the swimmer depends on how fast the cycle is executed, which depends linearly on the expansion rates of the spheres and connecting rod, as shown by equation (A.3).

The above results by Avron *et al* do not account for any hydrodynamic interaction between the spheres. The leading-order effect due to the interaction can be incorporated into the model by modifying equations (A.5) and (A.6) as

$$U_1 = \frac{F_1}{6\pi\mu a_1} + \frac{F_2}{4\pi\mu\ell} + \frac{a_1^2}{\ell^2}\dot{a}_1, \tag{A.5}$$

$$U_2 = \frac{F_1}{4\pi\mu\ell} + \frac{F_2}{6\pi\mu a_2} + \frac{a_2^2}{\ell^2}\dot{a}_2, \tag{A.6}$$

to include the interaction terms. The modified instantaneous swimmer velocity then reads

$$\begin{aligned}\bar{U} &= \frac{a_1 - a_2}{2(a_1 + a_2)}\dot{\ell}\left[\frac{1}{1 - \frac{3a_1a_2}{\ell(a_1+a_2)}}\right] + \frac{a_1^2}{\ell^2}\dot{a}_1,\\ &\sim \frac{a_1 - a_2}{2(a_1 + a_2)}\dot{\ell}\left[1 + \frac{3a_1a_2}{\ell(a_1 + a_2)} + \cdots\right] + \frac{a_1^2}{\ell^2}\dot{a}_1,\end{aligned} \tag{A.7}$$

upon expansion assuming $a_i \ll \ell$, which reproduces the leading-order correction obtained by Wang & Othmer [52]. When the swimmer performs the strokes described in figure 1(b) for a cycle, the net displacement with leading-order correction due to hydrodynamic interaction is given by

$$X \sim \frac{R-1}{R+1}\Delta\ell\left[1 + \frac{3a_sR}{(R+1)\Delta\ell}\ln(\ell_L/\ell_s)\right], \tag{A.8}$$

which shows an enhancement compared with the case when hydrodynamic interaction is absent (equation (A.4)).

ORCID iDs

I E Araci https://orcid.org/0000-0002-1327-9229

References

[1] Childress S 1981 *Mechanical of Swimming and Flying* (Cambridge: Cambridge University Press)
[2] Vogel S 1994 *Life in Moving Fluids* (Princeton, NJ: Princeton University Press)
[3] Fish F E and Lauder G V 2006 Passive and active flow control by swimming fishes and mammals *Annu. Rev. Fluid Mech.* **38** 193–224

[4] Gazzola M, Argentina M and Mahadevan L 2014 Scaling macroscopic aquatic locomotion *Nat. Phys.* **10** 758–61
[5] Purcell E M 1977 Life at low Reynolds number *Am. J. Phys.* **45** 3–11
[6] Lauga E 2011 Life around the scallop theorem *Soft Matter* **7** 3060–5
[7] Ebbens S J and Howse J R 2010 In pursuit of propulsion at the nanoscale *Soft Matter* **6** 726–38
[8] Gao W and Wang J 2014 The environmental impact of micro/nanomachines: a review *ACS Nano* **8** 3170–80
[9] Elgeti J, Winkler R G and Gompper G 2015 Physics of microswimmers—single particle motion and collective behavior: a review *Rep. Prog. Phys.* **78** 056601
[10] Hu C, Pané S and Nelson B J 2018 Soft micro- and nanorobotics *Annu. Rev. Control Robot. Auton. Syst.* **1** 53–75
[11] Nelson B J, Kaliakatsos I K and Abbott J J 2010 Microrobots for minimally invasive medicine *Annu. Rev. Biomed. Eng.* **12** 55–85
[12] Gao W and Wang J 2014 Synthetic micro/nanomotors in drug delivery *Nanoscale* **6** 10486–94
[13] Sengupta S, Ibele M E and Sen A 2012 Fantastic voyage: designing self-powered nanorobots *Angew. Chem., Int. Ed.* **51** 8434–45
[14] Fauci L J and Dillon R 2006 Biofluidmechanics of reproduction *Annu. Rev. Fluid Mech.* **38** 371–94
[15] Lauga E and Powers T R 2009 The hydrodynamics of swimming microorganisms *Rep. Prog. Phys.* **72** 096601
[16] Dreyfus R, Baudry J, Roper M L, Fermigier M, Stone H A and Bibette J 2005 Microscopic artificial swimmers *Nature* **437** 862–5
[17] Gao W, Sattayasamitsathit S, Manesh K M, Weihs D and Wang J 2010 Magnetically powered flexible metal nanowire motors *J. Am. Chem. Soc.* **132** 14403–5
[18] Pak O S, Gao W, Wang J and Lauga E 2011 High-speed propulsion of flexible nanowire motors: theory and experiments *Soft Matter* **7** 8169–81
[19] Zhang L, Abbott J J, Dong L, Peyer K E, Kratochvil B E, Zhang H, Bergeles C and Nelson B J 2009 Characterizing the swimming properties of artificial bacterial flagella *Nano Lett.* **9** 3663–7
[20] Ghosh A and Fischer P 2009 Controlled propulsion of artificial magnetic nanostructured propellers *Nano Lett.* **9** 2243–5
[21] Pak O S and Lauga E 2016 Theoretical models of low-Reynolds-number locomotion *Fluid-Structure Interactions in Low-Reynolds-Number Flows* (Cambridge, UK: The Royal Society of Chemistry) ch 4 pp 100–67
[22] Raz O and Avron J E 2007 Swimming, pumping and gliding at low Reynolds numbers *New J. Phys.* **9** 437
[23] Moran J L and Posner J D 2017 Phoretic self-propulsion *Annu. Rev. Fluid Mech.* **49** 511–40
[24] Barry N P and Bretscher M S 2010 Dictyostelium amoebae and neutrophils can swim *Proc. Natl Acad. Sci.* **107** 11376–80
[25] Bae A J and Bodenschatz E 2010 On the swimming of dictyostelium amoebae *Proc. Natl Acad. Sci.* **107** E165–6
[26] Farutin A, Rafaï S, Dysthe D K, Duperray A, Peyla P and Misbah C 2013 Amoeboid swimming: a generic self-propulsion of cells in fluids by means of membrane deformations *Phys. Rev. Lett.* **111** 228102
[27] Arroyo M, Heltai L, Millán D and DeSimone A 2012 Reverse engineering the euglenoid movement *Proc. Natl Acad. Sci.* **109** 17874–9
[28] Avron J E, Kenneth O and Oaknin D H 2005 Pushmepullyou: an efficient micro-swimmer *New J. Phys.* **7** 234
[29] Najafi A and Golestanian R 2004 Simple swimmer at low Reynolds number: three linked spheres *Phys. Rev.* E **69** 062901
[30] Dreyfus R, Baudry J and Stone H A 2005 Purcell's 'rotator': mechanical rotation at low Reynolds number *Eur. Phys. J.* B **47** 161–4
[31] Earl D J, Pooley C M, Ryder J F, Bredberg I and Yeomans J M 2007 Modeling microscopic swimmers at low Reynolds number *J. Chem. Phys.* **126** 064703
[32] Golestanian R and Ajdari A 2009 Stochastic low Reynolds number swimmers *J. Phys.: Condens. Matter* **21** 204104
[33] Alouges F, DeSimone A, Heltai L, Lefebvre-Lepot A and Merlet B 2012 Optimally swimming Stokesian robots *Discrete Continuous Dyn. Syst. - Ser.* B **18** 1189
[34] Alouges F, DeSimone A and Lefebvre A 2008 Optimal strokes for low Reynolds number swimmers: an example *J. Nonlinear Sci.* **18** 277–302
[35] Nasouri B, Vilfan A and Golestanian R 2019 Efficiency limits of the three-sphere swimmer *Phys. Rev. Fluids* **4** 073101
[36] Wang Q and Othmer H G 2016 Computational analysis of amoeboid swimming at low Reynolds number *J. Math. Biol.* **72** 1893–926
[37] Leoni M, Kotar J, Bassetti B, Cicuta P and Lagomarsino M C 2009 A basic swimmer at low Reynolds number *Soft Matter* **5** 472–6
[38] Grosjean G, Hubert M, Lagubeau G and Vandewalle N 2016 Realization of the Najafi-Golestanian microswimmer *Phys. Rev.* E **94** 021101
[39] Box F, Han E, Tipton C R and Mullin T 2017 On the motion of linked spheres in a Stokes flow *Exp. Fluids* **58** 29
[40] Klumpp S, Lefèvre C T, Bennet M and Faivre D 2019 Swimming with magnets: from biological organisms to synthetic devices *Phys. Rep.* **789** 1–54
[41] Yu T S, Lauga E and Hosoi A E 2006 Experimental investigations of elastic tail propulsion at low Reynolds number *Phys. Fluids* **18** 091701
[42] Espinosa-Garcia J, Lauga E and Zenit R 2013 Fluid elasticity increases the locomotion of flexible swimmers *Phys. Fluids* **25** 031701
[43] Liu B, Powers T R and Breuer K S 2011 Force-free swimming of a model helical flagellum in viscoelastic fluids *Proc. Natl Acad. Sci.* **108** 19516–20
[44] Gómez S, Godínez F A, Lauga E and Zenit R 2017 Helical propulsion in shear-thinning fluids *J. Fluid Mech.* **812** R3
[45] Tabak A F and Yesilyurt S 2012 Experiments on in-channel swimming of an untethered biomimetic robot with different helical tails *2012 4th IEEE RAS & EMBS Int. Conf. on Biomedical Robotics and Biomechatronics (BioRob)* (IEEE) pp 556–61
[46] Behkam B and Sitti M 2005 Modeling and testing of a biomimetic flagellar propulsion method for microscale biomedical swimming robots *Proc. of 2005 IEEE ASME Int. C. Adv.* 37–42
[47] Dasgupta M, Liu B, Fu H C, Berhanu M, Breuer K S, Powers T R and Kudrolli A 2013 Speed of a swimming sheet in newtonian and viscoelastic fluids *Phys. Rev.* E **87** 013015
[48] Saadat M, Mirzakhanloo M, Shen J, Tomizuka M and Alam M-R 2019 The experimental realization of an artificial low-Reynolds-number swimmer with three-dimensional maneuverability *2019 American Control Conf. (ACC)* (IEEE) pp 4478–84
[49] Kim M J, Bird J C, Van Parys A J, Breuer K S and Powers T R 2003 A macroscopic scale model of bacterial flagellar bundling *Proc. Natl Acad. Sci.* **100** 15481–5
[50] Grover J, Zimmer J, Dear T, Travers M, Choset H and Kelly S D 2018 Geometric motion planning for a three-link swimmer in a three-dimensional low Reynolds-number regime *2018 Annual American Control Conference (ACC)* (IEEE) pp 6067–74
[51] Zhang S, Or Y and Murray R M 2010 Experimental demonstration of the dynamics and stability of a low Reynolds number swimmer near a plane wall *Proc. of the 2010 American Control Conference* (IEEE) pp 4205–10
[52] Wang Q and Othmer H G 2018 Analysis of a model microswimmer with applications to blebbing cells and mini-robots *J. Math. Biol.* **76** 1699–763

[53] Happel J and Brenner H 1973 *Low Reynolds Number Hydrodynamics: With Special Applications to Particulate Media* (Groningen: Noordhoff)
[54] Hauser A W, Evans A A, Na J-H and Hayward R C 2015 Photothermally reprogrammable buckling of nanocomposite gel sheets *Angew. Chem., Int. Ed.* **54** 5434–7
[55] Huang H-W, Sakar M S, Petruska A J, Pané S and Nelson B J 2016 Soft micromachines with programmable motility and morphology *Nat. Commun.* **7** 12263
[56] Ohm C, Brehmer M and Zentel R 2010 Liquid crystalline elastomers as actuators and sensors *Adv. Mater.* **22** 3366–87
[57] Zeng H, Wasylczyk P, Parmeggiani C, Martella D, Burresi M and Wiersma D S 2015 Light-fueled microscopic walkers *Adv. Mater.* **27** 3883–7
[58] Palagi S *et al* 2016 Structured light enables biomimetic swimming and versatile locomotion of photoresponsive soft microrobots *Nat. Mater.* **15** 647
[59] Pozrikidis C 1994 *Boundary Integral and Singularity Methods for Linearized Viscous Flow* (Cambridge: Cambridge University Press)
[60] Shapere A and Frank W 1989 Geometry of self-propulsion at low Reynolds number *J. Fluid Mech.* **198** 557–85
[61] Tsang A C H, Tong P W, Nallan S and Pak O S 2020 Self-learning how to swim at low Reynolds number *Phys. Rev. Fluids* **5** 074101
[62] Tsang A C H, Demir E, Ding Y and Pak O S 2020 Roads to Smart Artificial Microswimmers *Adv. Intell. Syst.* **2** 1900137
[63] Cichos F, Gustavsson K, Mehlig B and Volpe G 2020 Machine learning for active matter *Nat. Mach. Intell.* **2** 94–103